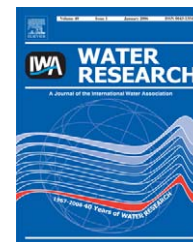


Available at www.sciencedirect.comjournal homepage: www.elsevier.com/locate/watres

Implications of a kinematic wave model for first flush treatment design

Joo-Hyon Kang^a, Masoud Kayhanian^b, Michael K. Stenstrom^{a,*}

^aDepartment of Civil and Environmental Engineering, University of California, Los Angeles, CA 90095-1953, USA

^bDepartment of Civil and Environmental Engineering, Center for Environmental and Water Resources Engineering, University of California, Davis, CA 95616, USA

ARTICLE INFO

Article history:

Received 15 February 2006

Received in revised form

26 August 2006

Accepted 5 September 2006

Available online 1 November 2006

Keywords:

Highway runoff

First flush

Stormwater

Kinematic wave equation

ABSTRACT

A deterministic model was developed to predict pollutant mass first flush and to utilize it for better design of best management practices (BMPs) that focus on treating the first flush. The model used the kinematic wave equation to calculate flow and mass transport, and erosion equations to calculate pollutant concentrations, which were assumed to be from a short and a long term source. The model parameters were calibrated with a parameter estimation procedure using three years' monitoring data from a highway runoff site in west Los Angeles. The simulation results showed that there exists an optimum watershed size to maximize first flush. Contours of watershed length, developed from simulations for different conditions of rainfall and watershed geometry, can be used to design runoff collection systems for highways and parking lots to maximize first flush.

© 2006 Elsevier Ltd. All rights reserved.

1. Introduction

Urbanized landuses generate greater stormwater volumes and runoff rates than undeveloped areas, possibly causing changes and degradation in receiving waters. The contaminant loads can be very high and are a function of landuse, with landuses having large vehicular traffic being among the highest sources (Barrett et al., 1998). Highways are essentially impervious and can have very high annual average daily traffic (AADT), and for this reason, are considered a major source for heavy metals, oil and grease and other toxic materials in stormwater runoff (Roger et al., 1998; Furumai et al., 2002; Kayhanian et al., 2003).

Pollutant washoff during a storm is commonly characterized by the existence of a first flush, popularly used to suggest the emission of a greater fraction of pollutant mass (mass first flush) or concentration (concentration first flush) in the early part of the runoff volume (Ma et al., 2002; Kim et al., 2005). The first flush phenomenon is frequently observed in the

runoff of small, highly impervious urbanized areas, such as highways and parking lots (Ma et al., 2002; Sansalone and Cristina, 2004). Therefore, characterizing the first flush phenomena is important to optimize treatment strategies. If a large portion of pollutant mass is contained in the first portion of the runoff, a BMP that is optimized to treat the first portion may be economically advantageous.

The first flush phenomenon is strongly related to hydrodynamic conditions as well as the geometry of the catchment. Numerous efforts have been performed to determine the relationship between pollutant washoff behavior and rainfall intensity, flow rate, watershed area or bottom slope, using statistical analysis of empirical observations (Gupta and Saul, 1996; Deletic and Maksimovic, 1998; Cristina and Sansalone, 2003a). Unfortunately no clear, general relationships have been found.

An alternative approach is to use deterministic models to investigate the dynamic behavior of contaminant washoff. A validated deterministic model could be used to evaluate

*Corresponding author. Tel.: +1 310 825 1408; fax: +1 310 206 5476.

E-mail address: stenstro@seas.ucla.edu (M.K. Stenstrom).

0043-1354/\$ - see front matter © 2006 Elsevier Ltd. All rights reserved.

doi:10.1016/j.watres.2006.09.007

| Nomenclature | | | |
|------------------|---|-----------|--|
| D | dispersion coefficient (m^2/s) | n | Manning's roughness coefficient |
| E | pollutant erosion rate from the bed surface ($g/m^2/s$) | m_b | pollutant mass available on the bed surface (g/m^2) |
| ε | erosion coefficient of pollutant (s/m^2) | $m_{b,t}$ | total pollutant mass on the bed surface (g/m^2) |
| ε_s | erosion coefficient of pollutant from the short-term source (s/m^2) | $m_{b,s}$ | pollutant mass from the short-term source on the bed surface (g/m^2) |
| ε_l | erosion coefficient of pollutant from the long-term source (s/m^2) | $m_{b,l}$ | pollutant mass from the long-term source on the bed surface (g/m^2) |
| ε'_l | redefined erosion coefficient of pollutant from the long-term source (gs/m^4) | m_w | pollutant mass in the water (g/m^2) |
| f | infiltration rate (cm/s) | p_p | pressure head (m) |
| h | flow depth (m) | S_0 | bed slope (fraction) |
| I | rainfall intensity (mm/h) | t | time (s) |
| K_p | hydraulic conductivity of the pavement (cm/s) | T | storm duration (h) |
| L | length of overland flow plane (m) | T_p | thickness of the pavement layer (m) |
| | | u | flow velocity (m/s) |
| | | u^* | friction velocity (m/s) |
| | | x | distance in the flow direction (m) |
| | | z | distance in the vertical direction (m) |

storm and catchment characteristics. If parameters relating to storm and catchment characteristics can be developed, they can be incorporated into a mathematical model, simulating the first flush in stormwater runoff to evaluate and optimize BMP design.

The objective of this study is to investigate the first flush phenomena in highway runoff as a function of the major characteristics of storms using a one-dimensional deterministic model that predicts both water quantity and quality. The design implications using the mass first flush simulation results are also discussed.

2. Background

2.1. First flush quantification

To quantify the high initial pollutant load of the first flush, Ma et al. (2002) suggested a concept of mass first flush (MFF) ratio as depicted in Fig. 1. Fig. 1 is created by plotting normalized discharged mass versus normalized runoff volume. The existence of a MFF can be determined if the data lie above the straight line, indicating a greater mass delivery in the early runoff volume. The intersection of a vertical line at a specific normalized volume and the mass line is used to calculate the MFF_n , by dividing the normalized mass at same normalized volume, designated as n , which is expressed as a percentage from 0 to 100%. For example, referring to Fig. 1, the MFF_{10} and MFF_{20} of a pollutant associated with 10% and 20% of the runoff volume are equal to 4.0 and 3.0, respectively (i.e., $MFF_{10} = 4.0$).

2.2. Deterministic models for rainfall-runoff

The simulation of temporal and spatial flow behavior can be performed by deterministic models such as the Saint-Venant system of equations and their simplifications. The Saint-Venant equations are composed of two conservative laws and have been popularly used for the open channel flow problems

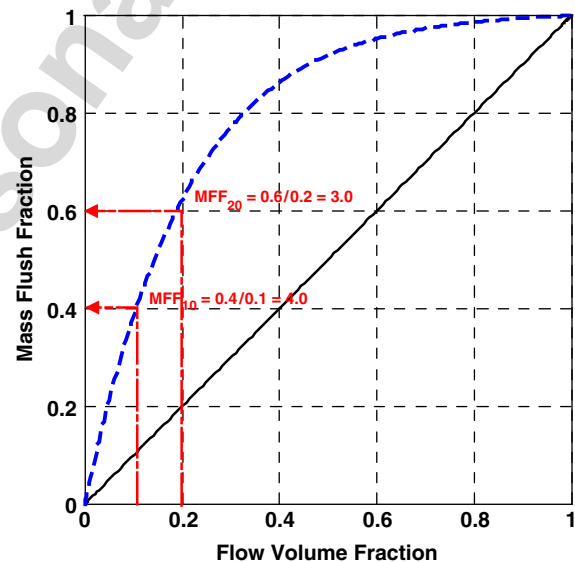


Fig. 1 – Definition of mass first flush ratio.

(Graf, 1998). The Saint-Venant equation can be reduced to the kinematic wave equation by neglecting local acceleration, convective acceleration and pressure force effects. The kinematic equation has been a preferred modeling equation for sheet flow over plane surfaces because the calculation is simple and accurate (Tomanovic and Maksimovic, 1996; Singh, 2002a, b; Cristina and Sansalone, 2003b).

The one-dimensional form of the kinematic wave equation, considering uniform rainfall and infiltration, is written on a unit width basis as follows:

$$\frac{\partial h}{\partial t} + mu \frac{\partial h}{\partial x} = 2.78 \times 10^{-8} I - 10^{-2} f, \tag{1}$$

$$u = (\sqrt{S_0}/n) \cdot h^{m-1}, \tag{2}$$

where h is flow depth (m), t is time (s), m is constant ($= 5/3$), u is flow velocity (m/s), x is distance in the flow direction (m), I

is rainfall intensity (mm/h), f is infiltration rate (cm/s), S_0 is bed slope, and n is Manning's roughness coefficient (The 2.78×10^{-8} conversion factor is needed when customary units are used for rainfall (mm/h) and infiltration (cm/s)). The initial and boundary conditions for the overland flow can be assumed as follows (Singh, 1996):

$$h(0, t) = 0, \quad t \geq 0, \quad (3)$$

$$h(x, 0) = 0, \quad 0 \leq x \leq L, \quad (4)$$

where L is length of overland flow plane (m).

Recently Tomanovic and Maksimovic (1996) and Singh (2002a, b) developed a deterministic model for solute discharge for different locations in a watershed for varying rainfall duration and hydraulic conditions using the kinematic wave equation. Previously, the majority of existing water quality models have been based on empirical or statistical approaches, due to a lack of mechanistic understanding.

3. Methodology

3.1. Model development

3.1.1. Infiltration

Although paved areas such as highways and parking lots are classified as "impervious" landuses, infiltration, albeit small, inevitably occurs. In this study, 10 cm-thick asphalt pavement is assumed to approximate infiltration rates through the road bed surfaces.

Introducing Darcy's law of permeability, infiltration rate can be expressed as

$$\begin{aligned} f &= -K_p \left(\frac{\partial h}{\partial z} \right) = -K_p \left(\frac{h + T_p - p_p}{T_p} \right), \\ &= -K_p \left(\frac{h - p_p}{T_p} \right) - K_p, \end{aligned} \quad (5)$$

where K_p is hydraulic conductivity of the pavement (cm/s), z is distance in the vertical direction (m), T_p is thickness of the pavement layer (m), and p_p is pressure head under the

pavement layer (m). Values of K_p of asphalt pavement has been generally reported in the range of 10^{-5} – 10^{-3} cm/s (Allen, 2003; Allen Cooley, 2003; Bowders et al., 2003). Assuming the pavement is asphalt supported by well draining materials such as gravel ($p_p = 0$), Eq. (5) can be reduced to a linear function of water flow depth (h) as follows:

$$f = -\frac{K_p}{T_p} h - K_p. \quad (6)$$

3.1.2. Pollutant transport

The advection–dispersion equation (ADE) is used for the mass pollutant transport calculation. Ignoring mass transfer through infiltration, the ADE is expressed as

$$\frac{\partial m_w}{\partial t} = \frac{\partial}{\partial x} \left(D \frac{\partial m_w}{\partial x} \right) - \frac{\partial}{\partial x} (u \cdot m_w) - E, \quad (7)$$

where m_w is pollutant mass in the water of the unit area (g/m^2), D is dispersion coefficient (m^2/s) and E is pollutant erosion rate from the bed surface ($\text{g}/\text{m}^2/\text{s}$).

The dispersion coefficient can be calculated using an equation developed for open channel flow (Elder, 1959) as follows:

$$D = 6.0hu^*, \quad (8)$$

where $u^* (= \sqrt{ghS_0})$ is friction velocity (m/s).

3.1.3. Pollutant erosion from plane surface

Pollutant erosion rate is generally assumed as a first-order reaction as a function of mass available on the bed surface (Singh, 1996; Tomanovic and Maksimovic, 1996). The erosion coefficient of solutes or cohesive particles is typically related to the bed shear stress, which is correlated with mean flow velocity (Chien and Wan, 1999). Therefore, the erosion equation can be formulated as.

$$E = \frac{dm_b}{dt} = -\varepsilon u^2 m_b, \quad (9)$$

where m_b is mass available on the bed surface (g/m^2) and ε is erosion coefficient (s/m^2).

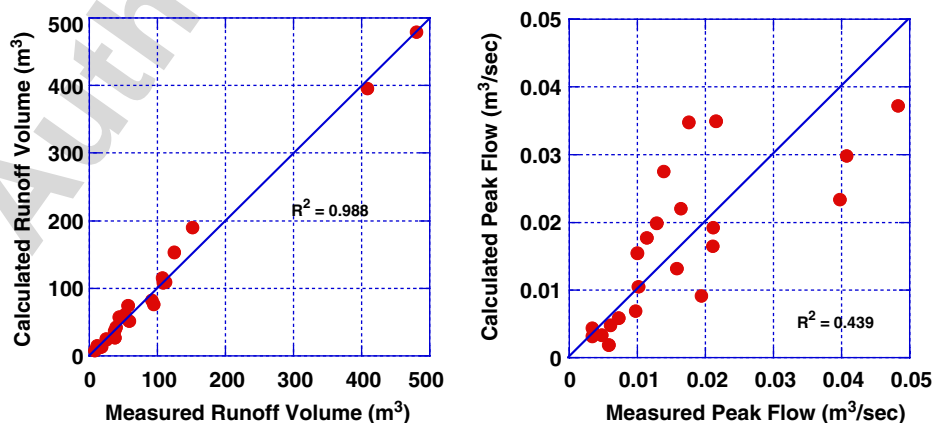


Fig. 2 – Relationships between measured and calculated flow volume and peak flows at $K_p = 10^{-5}$ cm/s (Values of R^2 are based on the line of equivalence).

Kim et al. (2005) and others (Bertrand-Krajewski et al., 1998) have shown that a pollutant is discharged with high concentration at the beginning of a storm (phase I), declining to a low concentration in a short time, followed by a prolonged residual concentration (phase II) to the end of the storm. Unfortunately Eq. (9) cannot properly model both the initial high pollutant concentrations observed in the early runoff and the low residual concentrations at the end of the storm (Kim et al., 2005; Deng et al., 2005). For example, over

the three years of monitoring the sites described in this study, it was not uncommon to observe chemical oxygen demand concentrations (COD) as high as 3000 mg/L at the beginning of a storm and as low as 20 mg/L at the end of the storm. This high/low or two-phase washoff was observed in most of the measured pollutants except suspended solids.

To model this two-phase phenomenon, two pollutant sources having different erosion rates were introduced: a “short-term” source and “long-term” source. The short-term

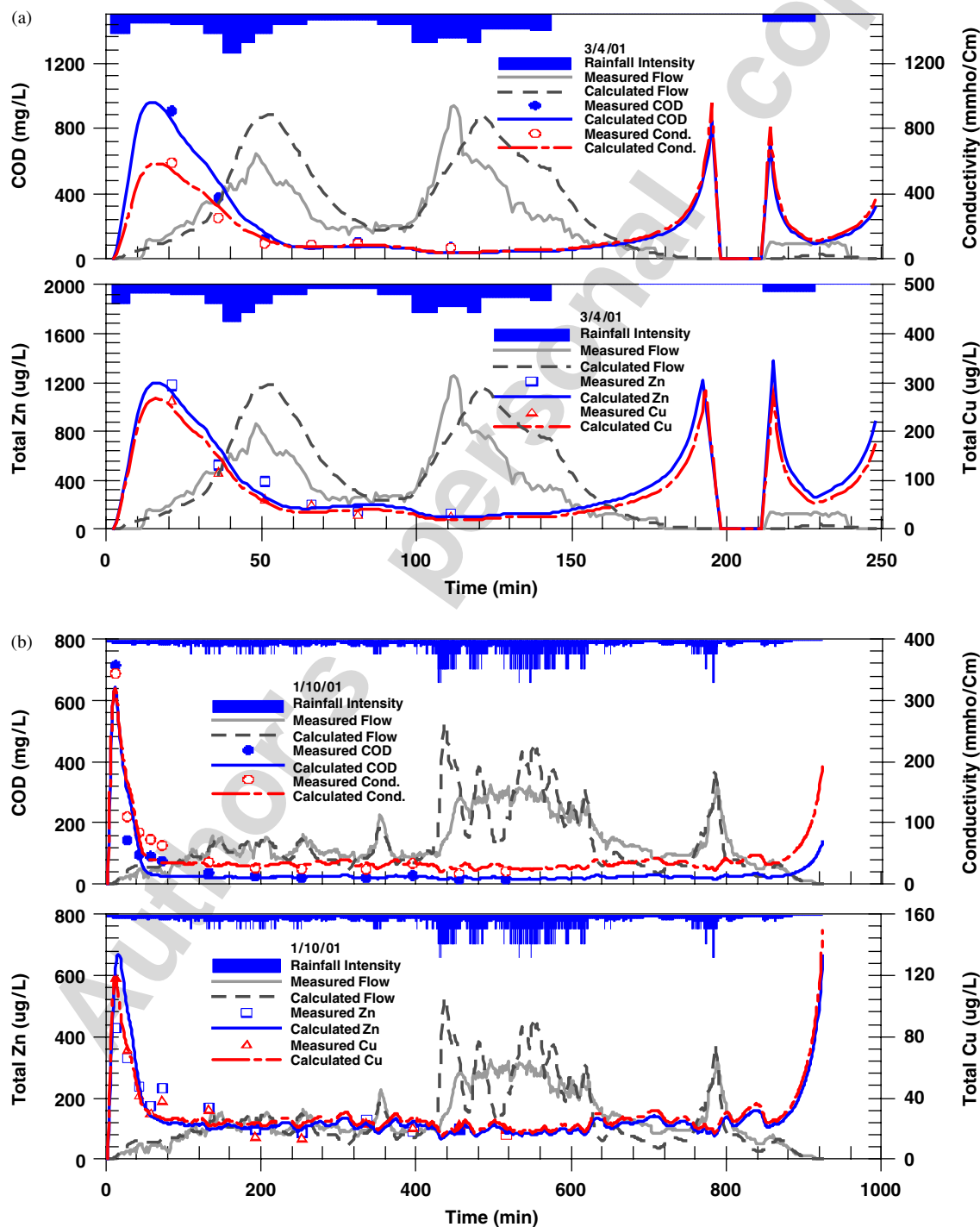


Fig. 3 – Measured and calculated hydrographs and pollutographs for two storm events: (a) 3/4/2001; (b) 1/10/2001.

source represents pollutant mass accumulated during antecedent dry days (ADD) before a storm. Pollutants from the short-term source are easily detached from the surface under even small flow energy because they are the top-most layer of the pollutant mass. In contrast, pollutants from the long-term source are not directly exposed to the flow shear or protected by the bed roughness. As a result, over repeated storm events, a fraction of pollutant survives and is solidified on the surface, acting as a semi-permanent pollutant source in the impervious watershed. The road itself can be considered as a long-term source generating various products of decomposition and aggregate materials (Sartor and Boyd, 1972). Considering the terms for two different pollutant sources, Eq. (9) can be modified as follows:

$$E = \frac{dm_{b,t}}{dt} = \frac{dm_{b,s}}{dt} + \frac{dm_{b,l}}{dt} = -\varepsilon_s u^2 m_{b,s} - \varepsilon_l u^2 m_{b,l}, \quad (10)$$

where $m_{b,t}$ is total pollutant mass per area (g/m^2), $m_{b,s}$ is pollutant mass per area from the short-term source (g/m^2), $m_{b,l}$ is pollutant mass per area from the long-term source (g/m^2), and ε_s and ε_l are erosion coefficients (s/m^2). For the case when the long-term mass does not appreciably change ($dm_{b,l}/dt \approx 0$) during a single storm, Eq. (10) can be simplified by redefining $\varepsilon_l m_{b,l}$ as a new coefficient (ε_l'), which is constant. This also simplifies the number of model parameters to be estimated. Then, Eq. (10) can then be written as

$$E = \frac{dm_{b,t}}{dt} = \frac{dm_{b,s}}{dt} = -\varepsilon_s u^2 m_{b,s} - \varepsilon_l' u^2, \quad (11)$$

ε_s (s/m^2) and ε_l' ($\text{g}/\text{s}/\text{m}^4$) are defined as erosion coefficients of pollutant mass from the short-term and long-term sources, respectively.

3.2. Site description

The monitoring site was located in west Los Angeles, near the UCLA campus. The catchment is a 21.9-m-wide and 178-m-long rectangular-shaped highway landuse. The average longitudinal slope is 0.02 north to south with little local variation, and only one storm-drain inlet exists on the highway shoulder at the south-most end of the site. Traffic loading is 322,000 annual average daily traffic (AADT, vehicles per day) and the average rainfall is approximately 330 mm/yr. The site was equipped with an automatic flow meter (American Sigma, model 950, Loveland, Colorado), a tipping bucket rain gauge and a composite auto sampler. Additional 4L grab samples were collected from a free water fall of the storm drain inlet. Additional information about the sites, monitor-

ing equipment and protocols has already been reported by Kim et al. (2005).

3.3. Calculation methods

The site was modeled as a 1-D catchment with a total length of 178 m. The measured rainfall data were used as the input rainfall and were assumed homogeneous along the distance. Flow was calculated on the basis of unit width and then multiplied by the site width (21.9 m) to be compared with the measured flow data.

The kinematic wave equation and transport equation were solved by the method of characteristics (Wood, 1993) and Crank–Nicolson method, respectively. Data from 22 storm events during 2000–2003 were used for the water quantity calculation and 12 storm events among them were available for the water quality parameter calibration.

A value of 0.011 was used for Manning's roughness coefficient (n) assuming that the pavement surface is made of smooth asphalt or concrete and a good fit was obtained when comparing measured and calculated flows for 22 storm events. The results were relatively insensitive to the value of n , with little degradation in the quality of the fit with $n = 0.014$, which is the larger normally used value of n (Bedient and Huber, 1992). Three values of K_p (i.e., 5×10^{-4} , 10^{-5} , and 2×10^{-5} cm/s) were evaluated to estimate a site-representative K_p . The value of 10^{-5} cm/s was best and used in the subsequent water quality calibrations for 12 storm events. Estimates of the water quality parameters, $m_{b,s}$ ($m_{b,s}^0$), ε_s and ε_l' ,

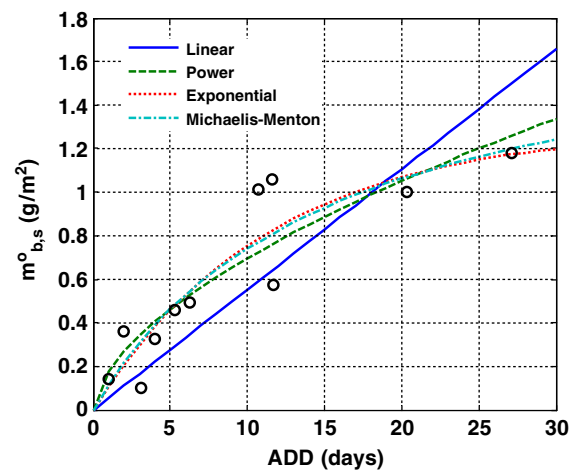


Fig. 4 – Regressions for COD buildup.

Table 1 – Range of calibrated water quality parameters

| Parameters | $m_{b,s}^0$ | ε_s^a | $\varepsilon_l'^b$ | R^{2c} |
|--------------|------------------------------------|--------------------------------------|--|----------|
| COD | 0.10–1.18 g/m^2 | 1.09 (0.6–1.2) s/m^2 | 0.0024 (0.001–0.004) $\text{g}/\text{s}/\text{m}^4$ | 0.92 |
| Conductivity | 0.10–0.55 $\mu\text{mho}/\text{m}$ | 0.99 (0.4–1.2) s/m^2 | 0.0027 (0.002–0.004) $\mu\text{mho}/\text{s}/\text{m}$ | 0.87 |
| Zn | 0.05–1.46 mg/m^2 | 0.87 (0.4–1.2) s/m^2 | 0.0073 (0.004–0.014) $\text{mg}/\text{s}/\text{m}^4$ | 0.95 |
| Cu | 0.05–0.29 mg/m^2 | 0.88 (0.4–1.2) s/m^2 | 0.0016 (0.001–0.0028) $\text{mg}/\text{s}/\text{m}^4$ | 0.90 |

^{a,b}Average values of 12 storm events with lower and upper boundaries in parentheses.

^c R^2 based on the line of equivalence between measured and modeled concentrations using 110 data points from 12 storm events.

were calculated for each storm event. A non-linear least-squares solver (i.e., “lscurvefit”) in the MATLAB toolbox was used to minimize the summation of error squares between measured and calculated pollutant concentrations.

4. Results and discussion

4.1. Flow calculation

Fig. 2 shows the calculated and measured runoff volumes and peak flow rates at $K_p = 10^{-5}$ cm/s, which was the best value among the three values of K_p evaluated (5×10^{-6} , 10^{-5} , and 2×10^{-5} cm/s). The values of R^2 were calculated based on the line of equivalence (sometimes known as the Nash-Sutcliffe, 1970 coefficient) to evaluate results. The results are relatively insensitive to the values of K_p evaluated and the flow model predicts runoff volume very well with R^2 larger than 0.98. The

fit between calculated and measured peak flows were more scattered when compared to the fit between calculated and measured runoff volume, but was reasonably simulated ($R^2 = 0.44$) in the evaluated range of K_p (5×10^{-6} – 2×10^{-5} cm/s). Based on the results presented in Fig. 2. A K_p value of 10^{-5} cm/s was chosen as the best site-representative for hydraulic conductivity.

Fig. 3 shows the hydrographs for two different storm events using K_p value of 10^{-5} cm/s. As can be seen, the 1-D runoff model simulates the measured peak flow rate, peak flow time and hydrodynamic flow patterns well.

4.2. Water quality parameter calibration

Calculated concentrations were fitted with measured concentrations to calibrate the model parameters ($m_{b,s}^0$, ϵ_s and ϵ'_j) for COD, conductivity, Zn and Cu, respectively for individual

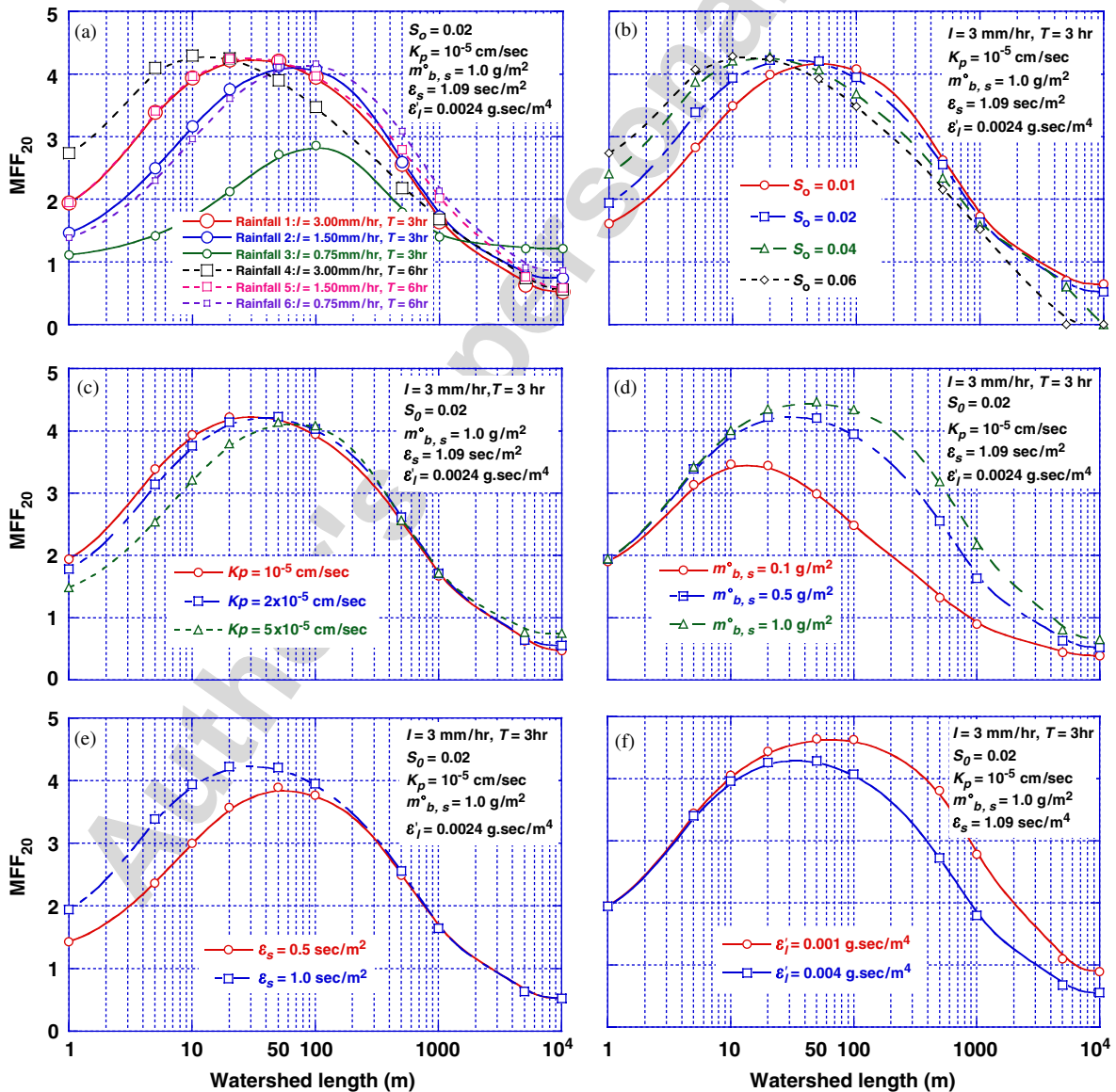


Fig. 5 – MFF₂₀ with respect to the watershed length for different factors: (a) I and T; (b) S_0 ; (c) K_p ; (d) $m_{b,s}^0$; (e) ϵ_s ; (f) ϵ'_j .

storm events. During the calibration, parameters were constrained to reasonable values by observing the measured and calculated concentration curves. Table 1 shows the calibrated parameters for different pollutants. The value of ϵ_s ranged from 0.87–1.10 s/m², without large variance among pollutants. The values of ϵ'_i , however, vary widely among different pollutants, which probably reflect the differences in long-term mass accumulation. As anticipated, the value of $m_{b,s}^0$ was different for individual storm events due to different ADDs.

Table 2 – Qualitative relationship between model variables and MFF_{20, max} and WL_{opt}

| Increasing model variables | MFF _{20, max} | WL _{opt} |
|----------------------------|------------------------|-------------------|
| I | ++ | -- |
| T | ++ | -- |
| S ₀ | + | -- |
| K _p | - | ++ |
| $m_{b,s}^0$ | + | ++ |
| ϵ_s | + | -- |
| ϵ'_i | - | -- |

+ Means increases, ++ means greater increase, - means decreases, -- means greater decrease.

Concentrations for each pollutant were calculated using calibrated parameters and plotted along with measured concentrations as shown in Fig. 3. The pollutant concentrations against time, shown in Fig. 3, illustrate pollutographs for two storm events. As can be seen, two-phase washoff phenomenon was fairly simulated with high R² values (based on the line of equivalence) between measured and calculated concentrations (Table 1) for all of the pollutants simulated. A quick rise in the calculated concentration sometimes occurs at the end of rainfall due to the reduced dilution caused by the flow decrease. To avoid infinite values of pollutant concentration in the runoff, the minimum flow rate required for the pollutant transport was set to 10⁻⁷ m³/s in the calculation. As a practical matter, the model is no longer useful at the end of a storm event and the simulations should be terminated before the end of the storm event.

4.3. Pollutant buildup

Using calibrated $m_{b,s}^0$ values for each storm event, buildup equations were evaluated and are shown in Fig. 4. This figure illustrates COD buildup as a function of ADD, showing the plots of calibrated values of $m_{b,s}^0$ fitted with four different curve forms using the least-squares method. The linear equation has

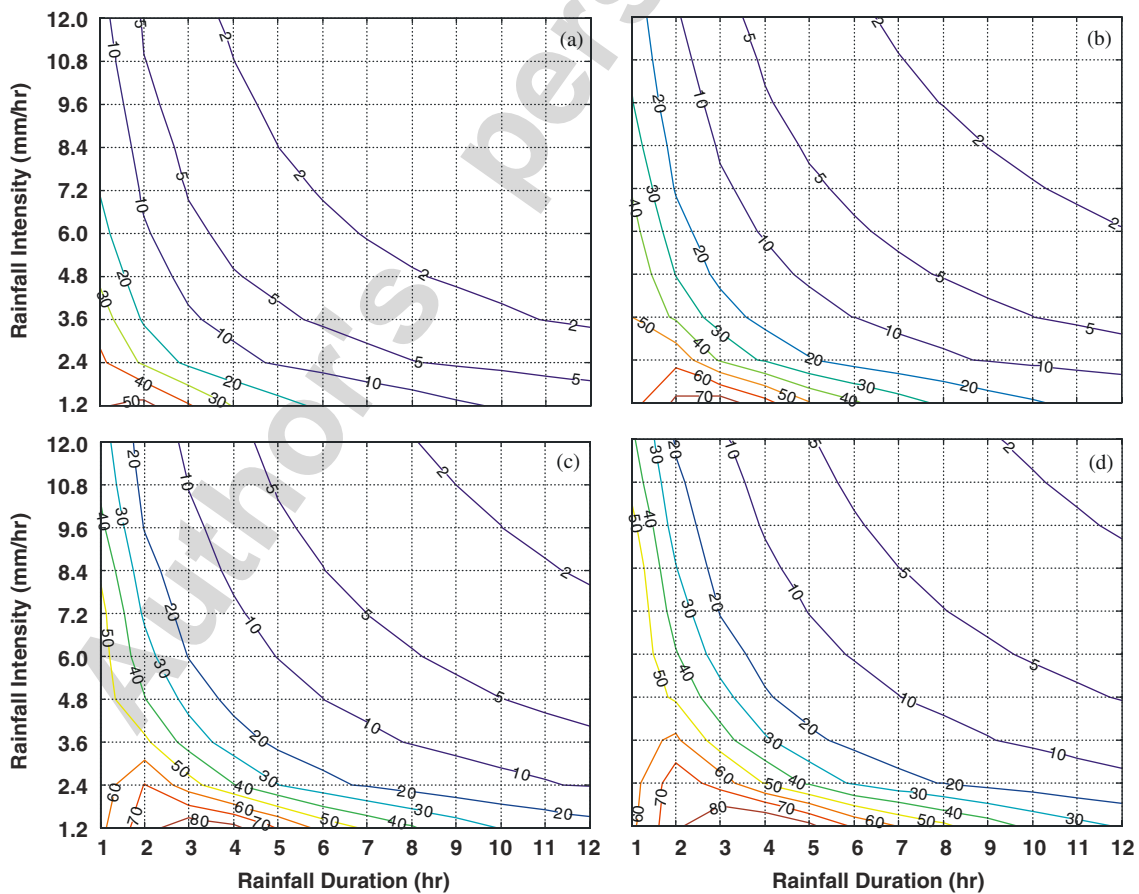


Fig. 6 – Contours of the optimal watershed length at S₀ = 0.02 for different values of m_{b,s}⁰: (a) 0.1 g/m²; (b) 0.5 g/m²; (c) 1.0 g/m²; (d) 1.5 g/m².

the poorest fit and the other three equations provide similar fits. The choice of equation may be related to the intended use of the model, with applications dominated by lower ADD using a different buildup equation than applications dominated by longer ADD. COD is shown in Fig. 4, but formulas for the other pollutants were also obtained in the same manner, although they are not presented in this paper.

4.4. First flush simulations

Calibrated model parameters for COD were used for the MFF simulations. MFF_{20} was selected as the representative MFF ratio and investigated as a function of watershed length (WL) under different conditions in rainfall intensity, rainfall duration, slope, pavement hydraulic conductivity, initial mass and erosion coefficients. Constant rainfall intensity was assumed for the input rainfall. MFF_{20} was calculated at several discrete points of WL and interpolated to produce a continuous function for graphing.

4.5. Maximum MFF ratio and optimum watershed length

The MFF simulation results reveal an optimum watershed length (WL_{opt}) that maximizes MFF_n . Extremely small or large

watersheds cannot have high MFF_n . In a small watershed, runoff rapidly flushes out without forming sufficiently high flow rate; as a result, pollutants are not well mobilized due to lack of flow energy. In a very large watershed, pollutants travel a long distance, resulting in retardation of mass emission although large flow energy effectively erodes pollutants from the surface. MFF could be even inverted ($MFF_n < 1.0$) in an extremely large watershed.

4.6. Relationship between MFF and site and rainfall conditions

Six hypothetical rainfalls with different rainfall intensity and duration were simulated and calculated values of MFF_{20} were plotted as functions of WL in Fig. 5(a). As can be seen, Maximum MFF_{20} ($MFF_{20, max}$) occurs at different WLs for each rainfall simulated. This is because different combinations of rainfall intensity and duration change hydraulic conditions, resulting in different emission rates of pollutants. Higher rainfall intensity and longer duration produce larger MFF_{20} and smaller WL_{opt} .

Fig. 5(b) displays the effect of the bed slope on MFF_{20} . As the slope increases, WL_{opt} becomes shorter. $MFF_{20, max}$ proportionally increases as the slope increases although the increments were small in the simulated slope range (0.01–0.06).

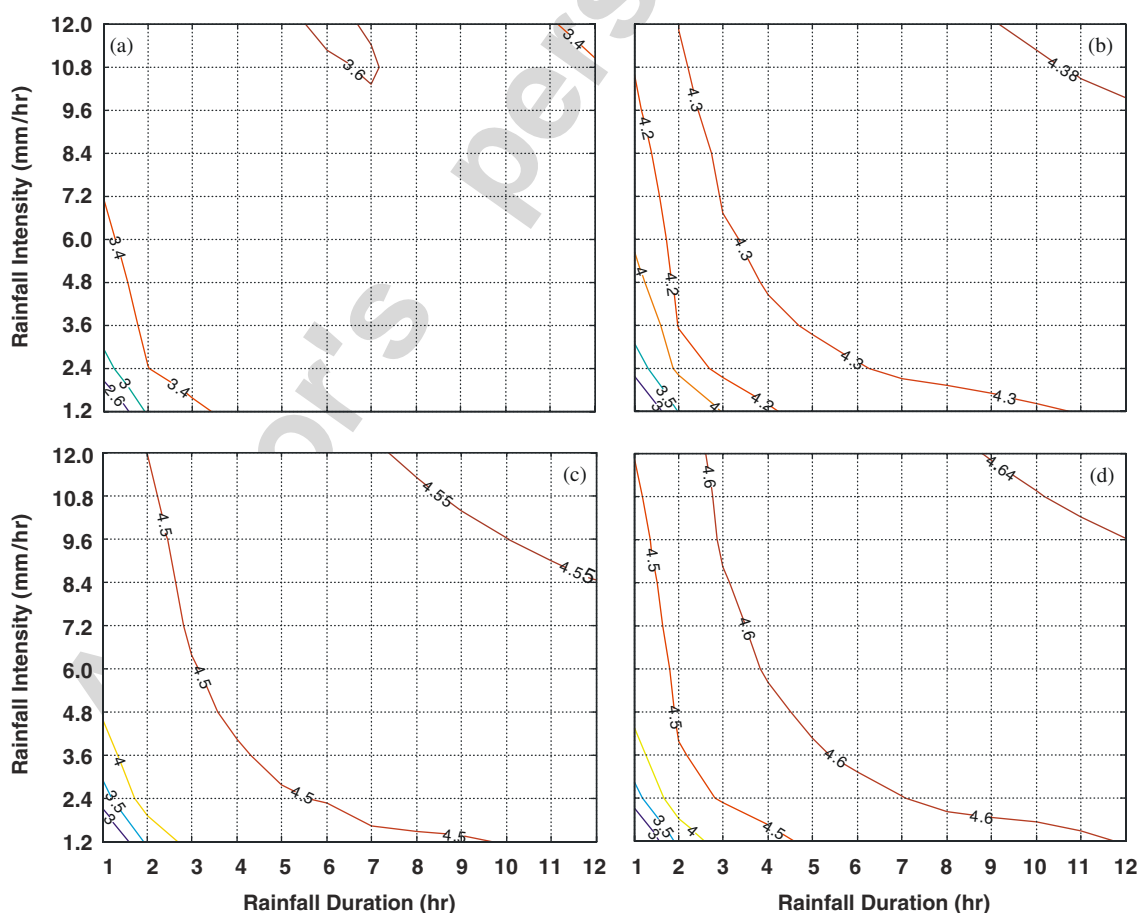


Fig. 7 – Contours of the maximum MFF_{20} at $S_0 = 0.02$ for different values of $m_{b,s}$: (a) 0.1 g/m^2 ; (b) 0.5 g/m^2 ; (c) 1.0 g/m^2 ; (d) 1.5 g/m^2 .

Fig. 5(c) shows MFF_{20} with respect to WL for three different values of K_p ranging from 10^{-5} to 5×10^{-5} cm/sec. As can be seen, smaller K_p produces larger MFF_{20} , and shorter WL_{opt} . $MFF_{20, max}$ also decreases as K_p increases. High infiltration rate reduces net precipitation, thereby retarding pollutant erosion rate because of lower flow energy. MFF_{20} becomes less sensitive to the infiltration rate for long watersheds ($WL > 300$ m).

Different values of $m_{b,s}^0$ were simulated in Fig. 5(d). Larger $m_{b,s}^0$ yields larger MFF_{20} and WL_{opt} . $m_{b,s}^0$ strongly affects the MFF_{20} in large watersheds. In contrast, the differences among the values of MFF_{20} for different values of $m_{b,s}^0$ were small in a very small watershed ($WL < 10$ m). With $m_{b,s}^0$ larger than 1.0 g/m², there was little change in MFF_{20} curves. In this case, the short-term source becomes the dominant pollutant source, so that the total mass emission rate is primarily controlled by ϵ_s , not the absolute amount of total pollutant mass. As the ADD increases, the short-term pollutant accumulation approaches a maximum capacity. Therefore, the relationship between MFF and ADD becomes weaker as the ADD increases because of limited mass accumulation as well as domination of the short-term source in the total pollutant mass.

Fig. 5(e) shows the simulation results of MFF_{20} using two different values of ϵ_s . Higher ϵ_s produces greater MFF_{20} but smaller WL_{opt} . The impact of ϵ_s on MFF_n diminishes in a

relatively long watershed and Fig. 5(e) shows that values of $\epsilon_s = 0.5$ s/m² and $\epsilon_s = 1.0$ s/m² produce essentially the same MFF_{20} in watersheds longer than approximately 200 m. Fig. 5(f) shows the effect of ϵ'_1 , and MFF_{20} is very sensitive to the change of ϵ'_1 in the long watersheds. For shorter watersheds, the sensitivities to ϵ_s and ϵ'_1 are reversed.

4.7. Implications for BMP design

Conditions to obtain higher MFF ratios can be determined through simulations which change the size of the drainage areas or use multiple drain inlets. The MFF simulations shown in Fig. 5 provide a qualitative relationship between the MFF ratio and affecting factors as summarized in Table 2. This qualitative result might be useful as a screening tool before undertaking field BMP design and construction. A universal design procedure will not be possible because of site specific conditions, due to the diversity in slope, rainfall and available mass of pollutant. Fig. 5 also shows the design conditions to use in the event that a first flush is not desired (i.e., no BMP is provided or it is desired to minimize peak concentrations to receiving waters).

MFF_{20} was evaluated as a design parameter assuming 20% of total runoff volume is treated. The broad peak of simulated MFF ratios implies a wide range of lengths to obtain high or favorable

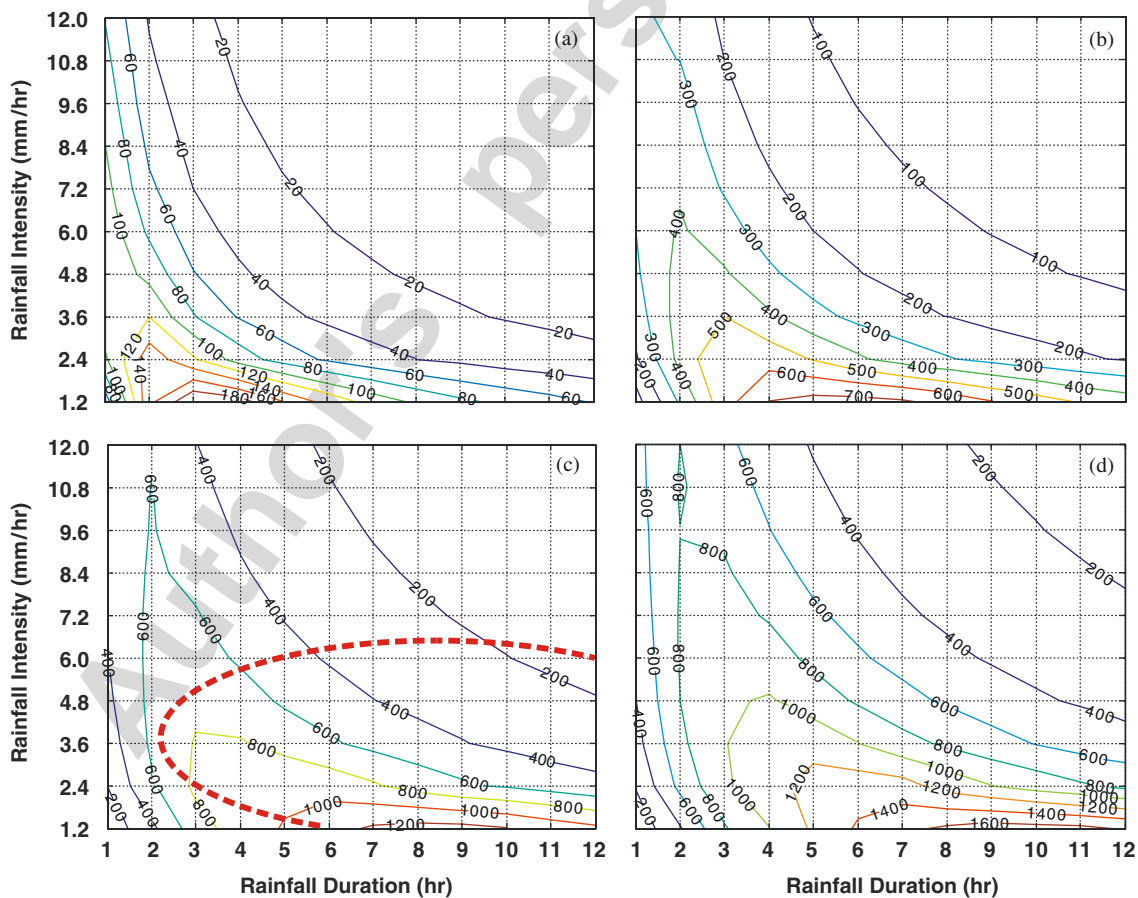


Fig. 8 – Contours of the maximum watershed length at $MFF_{20} = 2.5$ and $S_0 = 0.02$ for different values of $m_{b,s}^0$: (a) 0.1 g/m²; (b) 0.5 g/m²; (c) 1.0 g/m²; (d) 1.5 g/m². Ellipse in (c) shows the region corresponding to the mean values of observed rainfall intensity and duration surrounded by 1 standard deviation.

MFF ratios (see Fig. 5). A strategy in determining a design WL (WL_{des}) can be selecting a value between WL_{opt} and the WL at a required MFF_{20} , which is the upper limit of allowable WL.

Using the calibrated model parameters for COD, comprehensive MFF simulations were conducted to generate a design tool for determining the watershed length. Fig. 6 shows contours of WL_{opt} as a function of rainfall intensity and duration for different $m_{b,s}^0$ values at $S_0 = 0.02$. Contours of $MFF_{20, max}$ corresponding to the WL_{opt} were also constructed as shown in Fig. 7. Similarly, Fig. 8 illustrates contours of the maximum WL at $MFF_{20} = 2.5$ (if $MFF_{20, max} < 2.5$, $MFF_{20, max}$ was used in the contours).

These contours can be used to select a WL_{des} . For example, Fig. 6(c) and Fig. 8(c) can be used to determine WL for 0.02 of slope and 1.0 g/m^2 of $m_{b,s}^0$ for the studied site. The value of $m_{b,s}^0$ was calculated using the exponential buildup formula obtained in Fig. 4 and based on 17 days ADD, which is the average ADD during wet season over the 3 years of observations. The ellipse in Fig. 8(c) shows the region corresponding to the mean values of observed rainfall intensity and duration ($I = 3.8 \text{ mm/h}$, $T = 8.2 \text{ h}$) surrounded by 1 standard deviation that were observed using 3 years' monitoring data at the site. A design WL can be selected inside the ellipse.

5. Conclusions

A one-dimensional deterministic model for predicting mass first flush runoff was developed and calibrated using 22 storms from 3 years of observations at a high-traffic volume highway site (AATD $\sim 300,000$). The model uses the kinematic wave equation and assumes a short and long term pollutant source. The model predicts both runoff rate and pollutant concentrations for selected pollutants (COD, total zinc, total copper and conductivity) until the end of the storm event, when runoff rate declines to zero. The following conclusions are made:

- Calibrated initial mass of the short-term source was fitted with different types of buildup formulas, and correlated well with ADD.
- qualitative relationships between MFF and site characteristics such as rainfall intensity, duration, infiltration rate, slope, initial mass, erosion coefficients and watershed length were obtained using the developed 1-D deterministic model.
- Mass first flush simulations revealed that there exists an optimum watershed length for maximizing the first flush. Therefore, catchment sizes can be selected to maximize the first flush or the MFF ratio.
- Contours of watershed length generated by a family of MFF simulations can be used in determining locations and number of storm-drain inlets to maximize the first flush for highway BMPs.

Acknowledgments

This study was supported in part by California Department of Transportation (Caltrans), Division of Environmental

Analysis. The authors are grateful to their continuous support.

REFERENCES

- Allen, D.L., 2003. Analysis of field permeability and laboratory shear stresses for western Kentucky parkway milepost 18.240 to milepost 25.565 Caldwell-Hopkins Counties. Research Report, KTC-03-05/SPR245-02-1I, Kentucky Transportation Center, University of Kentucky, Lexington Kentucky.
- Allen Cooley Jr., L., 2003. Evaluation of pavement permeability in Mississippi. National Center for Asphalt Technology. Auburn University, Auburn, Alabama.
- Barrett, M.E., Irish Jr., L.B., Malina Jr., J.F., Charbeneau, R.J., 1998. Characterization of highway runoff in Austin, Texas, Area. *J. Environ. Eng., ASCE* 124 (2), 131–137.
- Bedient, P.B., Huber, W.C., 1992. Hydrology and Floodplain Analysis. Addison-Wesley Publishing Company, USA.
- Bertrand-Krajewski, J.-L., Chebbo, G., Saget, A., 1998. Distribution of pollutant mass vs volume in stormwater discharges and the first flush phenomenon. *Water Res.* 32 (8), 2341–2356.
- Bowders, J.J., Blanco, A.M., Parra, J.R., 2003. Characterization of permeability of pavement bases in Missouri Department of Transportation's System. Final Report, RDT 03-005, Research Investigation 01-006, Missouri Department of Transportation Research, Development and Technology, Jefferson City, Missouri.
- Chien, N., Wan, Z., 1999. Mechanics of Sediment Transport. ASCE Press, Reston, Virginia.
- Cristina, C.M., Sansalone, J.J., 2003a. First flush, power law and particle separation diagrams for urban storm-water suspended particulates. *J. Environ. Eng. ASCE* 129 (4), 298–307.
- Cristina, C.M., Sansalone, J.J., 2003b. Kinematic wave model of urban pavement rainfall-runoff subject to traffic loadings. *J. Environ. Eng. ASCE* 129 (7), 629–636.
- Deletic, A.B., Maksimovic, C.T., 1998. Evaluation of water quality factors in storm runoff from paved areas. *J. Environ. Eng. ASCE* 124 (9), 869–879.
- Deng, Z.Q., Lima, J.L.M.P., Singh, V.P., 2005. Fractional kinetic model for first flush of stormwater pollutants. *J. Environ. Eng. ASCE* 131 (2), 232–241.
- Elder, J.W., 1959. The dispersion of marked fluid in a turbulent shear flow. *J. Fluid Mech.* 5 (4), 544–560.
- Furumai, H., Balmer, H., Boller, M., 2002. Dynamic behavior of suspended pollutants and particle size distribution in highway runoff. *Water Sci. Tech.* 46 (11), 413–418.
- Graf, W.H., 1998. Fluvial Hydraulics: Flow and Transport Processes in Channels of Simple geometry. Wiley Inc., New York, USA.
- Gupta, K., Saul, A.J., 1996. Specific relationship for the first flush load in combined sewer lows. *Water Res.* 30 (5), 1244–1252.
- Kayhanian, M., Singh, A., Suverkropp, C., Borroum, S., 2003. Impact of annual average daily traffic on highway runoff pollutant concentrations. *J. Environ. Eng. ASCE* 129 (11), 975–990.
- Kim, L.-H., Kayhanian, M., Zoh, K.-D., Stenstrom, M.K., 2005. Modeling of highway stormwater runoff. *Sci. of Total Environ.* 348, 1–18.
- Ma, M., Khan, S., Li, S., Kim, L.-H., Ha, S., Kayhanian, M., Stenstrom, M.K., 2002. First flush phenomena for highways: how it can be meaningfully defined. *Proceedings of ninth International Conference on Urban Drainage*, September, Portland, Oregon.
- Nash, J.E., Sutcliffe, J.V., 1970. River flow forecasting through conceptual models part I-A discussion of principles. *J. Hydrol.* 10 (3), 282–290.

- Roger, S., Montréjaud-Vignoles, M., Andral, M.C., Herremans, L., Fortune, J.P., 1998. Mineral, physical and chemical analysis of the solid matter carried by motorway runoff water. *Water Res.* 32 (4), 1119–1125.
- Sansalone, J.J., Cristina, C.M., 2004. First flush concepts for suspended and dissolved solids in small impervious watersheds. *J. Environ. Eng. ASCE* 130 (11), 1301–1314.
- Sartor, J.D., Boyd, G.B., 1972. Water pollution, aspects of street surface contaminants. EPA-R2-72-081, USEPA.
- Singh, V.P., 1996. *Kinematic Wave Modeling in Water Resources: Surface Water Hydrology*. Wiley, New York.
- Singh, V.P., 2002a. Kinematic wave solutions for pollutant transport by runoff over an impervious plane, with instantaneous or finite-period mixing. *Hydrol. Process.* 16, 1831–1863.
- Singh, V.P., 2002b. Kinematic wave solutions for pollutant transport over an infiltrating plane with finite-period mixing and mixing zone. *Hydrol. Process.* 16, 2441–2477.
- Tomanovic, A., Maksimovic, C., 1996. Improved modeling of suspended solids discharge from asphalt surface during storm event. *Water Sci. Tech.* 33 (4–5), 363–369.
- Wood, W.L., 1993. *Introduction to Numerical Methods for Water Resources*. Oxford University Press, New York.

Author's personal copy